# Numerical simulation of the ultrasonic waves generated by ring-shaped laser illumination

**Zhonghua Shen (沈中华), Jianfei Guan (关建飞), Jian Lu (陆 建), and Xiaowu Ni (倪晓武)**

*Department of Applied Physics, Nanjing University of Science and Technology, Nanjing 210094*

The improvement of the generation efficiency has attracted much attention, confronted with the little amplitude of acoustic wave generated by pulsed laser in the thermoelastic regime. This paper constructed the finite element model to simulate ultrasonic waves generated by the ring-shaped laser source with the 8 mm inner radii. The numerical results demonstrate that strong focusing exists at the center axis of ring as the result of constructive interference of the waves generated by different parts of the source. Furthermore, the bulk wave includes compression, shear peak amplitudes and the surface acoustic wave magnitude drops quickly when the receiver position is away from the epicenter. Numerical simulations indicated that the low acoustic amplitudes in laser acoustics can be relieved somewhat by taking advantage of constructive interference between waves generated by different parts of an acoustic source, giving locally higher amplitude.

*OCIS codes*: 040.0040, 140.0140, 160.0160.

Optical technique for the generation and detection of ultrasound is well established and has been utilized in a wide variety of nondestructive evaluation (NDE) and materials characterization applications[1,2]. The technique of laser acoustic wave generation has the problem of producing relatively low acoustic amplitudes. The acoustic amplitude is limited because one usually wants to avoid melting or ablating the surface of the material under study. The usual photothermal generation mechanism in testing applications is based on the rapid and small thermal expansion of a heated surface layer[3]. There have been numerous reports of designing laser patterns, for either spatially or temporally tailored acoustic generation[4−9], they all demonstrated that the difficulty of low acoustic amplitudes in laser acoustics can be relieved somewhat by taking advantage of constructive interference between waves generated by different parts of an acoustic source, giving locally higher amplitude. The acoustic source is then a pattern of laser illumination designed in space and time. Littman[10] has report measurement of bulk ultrasonic waves generated in aluminum plates with irradiation of ring-shaped laser light. The literatures described the experimental procedure and discussed the results of experiments.

In this article we report the simulated results of bulk and surface ultrasonic waves generated in aluminum plates with irradiation of ring-shaped laser light by the finite element method (FEM), which is a series of computerized numerical calculations using a matrix method and is used in many fields, particularly mechanics and construction engineering, as a practical method for the simulation of thermal and elastic phenomena[11−13]. In this paper, a simulation of the process by laser-generated ultrasound is demonstrated using FEM. A detailed study of the displacement field generated by the bulk ultrasonic waves is provided.

The physical problem which we wish to consider is the structural response of a homogeneous, elastic, isotropic single plate system when a ring-shaped laser pulse impacts the surface of the sample. The geometry of the problem is shown in Fig. 1. The laser beam is assumed to be perpendicular to the surface, where it heats a finite subsurface volume. Since the geometry of the problem has axial symmetry, it is convenient to use a cylindrical coordinate system.

Due to the fact that the axial symmetry is characterized by the conditions: $u_\theta = 0$, $\frac{\partial u}{\partial \theta} = 0$, and the components $u_x = u_x(x, y, t)$, $u_y = u_y(x, y, t)$ are independent of $\theta$. Therefore, the theory model shown in Fig. 1 can be reduced to the model which is described in Fig. 2.

The classical thermal conduction equation for finite elements with the heat capacity matrix $[C]$, the conductivity matrix $[K]$, the heat flux vector $\{p_1\}$ and the heat source vector $\{p_2\}$ can be expressed as

$$[K]\{T\} + [C]\left\{\dot{T}\right\} = \{p_1\} + \{p_2\}, \tag{1}$$

where $\{T\}$ is the temperature vector, and $\{\dot{T}\}$ is the temperature rise rate vector.

For wave propagation, ignoring damping, the governing finite element equation is

$$[M]\{\ddot{\mathbf{U}}\} + [K]\{\mathbf{U}\} = \{\mathbf{F}_{\text{ext}}\}, \tag{2}$$

where $[M]$ is the mass matrix, $[K]$ is the stiffness matrix, $\{\mathbf{U}\}$ is the displacement vector, $\{\ddot{\mathbf{U}}\}$ is the acceleration vector and $\{\mathbf{F}_{\text{ext}}\}$ is the external force vector.

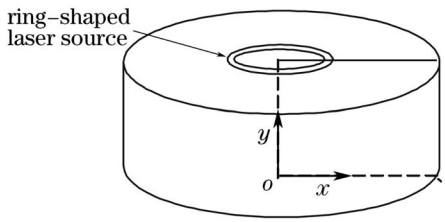


Fig. 1. Schematic diagram of the sample irradiated by ring-shaped laser.

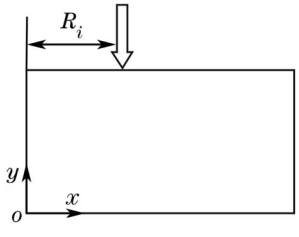


Fig. 2. Cross section of the sample.

For thermoelasticity, the external force vector for an element is $\int_{V_e}[B]^T[D]\{\varepsilon_0\}\mathrm{d}V$, where $\{\varepsilon_0\}$ is the thermal strain vector, $[B]^T$ is the transpose of the derivative of the shape functions and $[D]$ is the material matrix.

For the implementation of Eq. (2) an implicit time integration scheme based on Newmark's algorithm has been selected. Equation (2) is therefore converted into

$$\left([K]+\frac{1}{\alpha\Delta t^2}[M]\right)\{\mathbf{U}\}_t = \{\mathbf{F}_{\mathrm{ext}}\}+[M]\left[\frac{1}{\alpha\Delta t^2}\{\mathbf{U}\}_{t-\Delta t}+\frac{1}{\alpha\Delta t}\left\{\dot{\mathbf{U}}\right\}_{t-\Delta t}+\left(\frac{1}{2\alpha}-1\right)\left\{\ddot{\mathbf{U}}\right\}_{t-\Delta t}\right], \quad (3)$$

where the velocity and acceleration terms are given by

$$\left\{\ddot{\mathbf{U}}_{t-\Delta t}\right\}=\frac{1}{\alpha\Delta t^2}\left(\{\mathbf{U}_{t-\Delta t}\}-\{\mathbf{U}_{t-2\Delta t}\}\right)-\frac{1}{\alpha\Delta t}\left\{\dot{\mathbf{U}}_{t-2\Delta t}\right\}-\left(\frac{1}{2\alpha}-1\right)\left\{\ddot{\mathbf{U}}_{t-2\Delta t}\right\}, \quad (4)$$

$$\left\{\dot{\mathbf{U}}_{t-\Delta t}\right\}=\left\{\ddot{\mathbf{U}}_{t-2\Delta t}\right\}+\Delta t\,(1-\delta)\left\{\ddot{\mathbf{U}}_{t-2\Delta t}\right\}+\Delta t\delta\left\{\ddot{\mathbf{U}}_{t-\Delta t}\right\}. \quad (5)$$

By choosing $\delta=\frac{1}{2}$ and $\alpha=\frac{1}{4}$ the scheme becomes unconditionally stable; and through progressively integrating Eq. (3) over $n\Delta t$ (where $n=0,1,\cdots$, total number of time steps), the entire time history is generated.

Based on the above described theories, the thermoelastic generated waves are calculated in annular aluminum plates with 40-mm radius and 12.7-mm thickness, respectively. The laser energy is 13.5 mJ, the pulse rise time and the element size are taken to be 10 ns and 100 $\mu$m. Figure 3 shows the typical results of normal displacement waveforms occurred at the epicenter and the positions of 0.5, 1.0, and 1.5 mm off the epicenter, respectively.

In Fig. 3(a), a sharp rise at 2.4 $\mu$s represents the arrival of the compressional waves, followed by a peak with larger amplitude at 4.9 $\mu$s that represents the shear wave arrival. Two more features follow at 6.4 and 8.6 $\mu$s, which are due to reflections between the back and front surface of the sample. In Figs. 3(b) and (c), as the receiver points are away from the centre locations, the signal amplitude

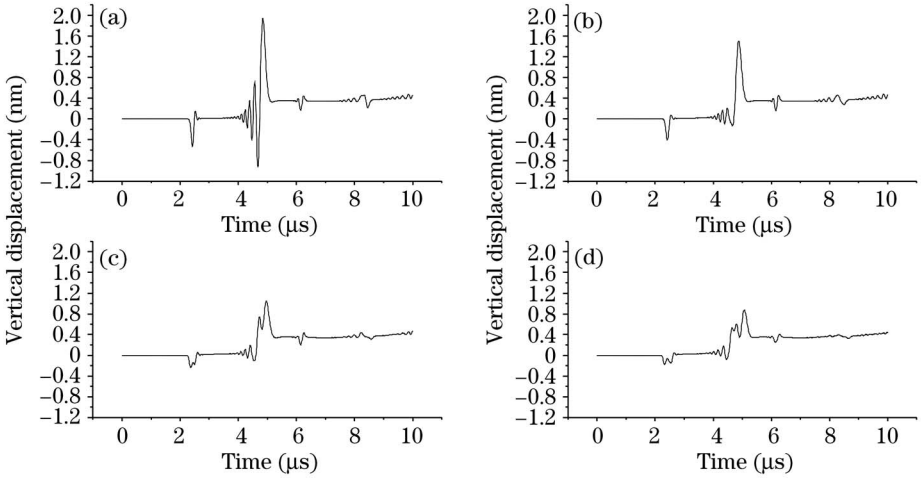


Fig. 3. Recorded rear surface wave forms for a 12.7-mm-thick aluminum plate illuminated by an 8-mm-radius ring. The recorded position is (a) the epicenter, (b) 0.5 mm, (c) 1 mm, (d) 1.5 mm from epicenter.

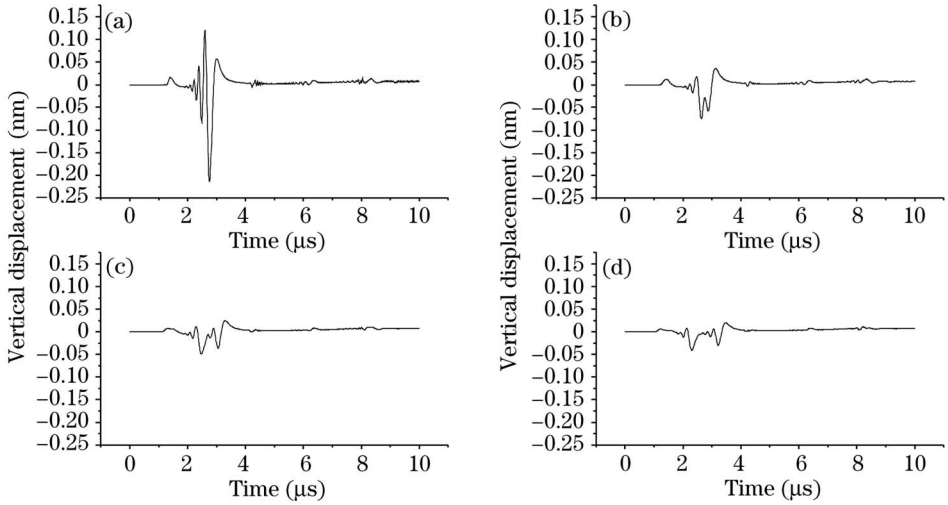


Fig. 4. Recorded top surface wave forms for a 20-mm-thick aluminum plate illuminated by an 8-mm-radius ring. The recorded position is (a) the center of the ring, (b) 0.5 mm, (c) 1 mm, (d) 1.5 mm from center.

drops rapidly, since waves are created by different portions of the ring no longer reinforced by arriving at the detector at the same time. Finally, in Fig. 3(d), for the sharp shear and compression peaks each splits into two separated peaks whose amplitudes are only 25% of that of the original peaks.

Meanwhile, it should be noted that the top surface acoustic wave also has similar tendency of the bulk wave recorded at the epicenter. From Figs. 4(b) and (c), as the receiver points are away from the centre locations, the signal amplitude drops rapidly, since waves are created by different portions of the ring that no longer reinforced by arriving at the detector at the same time. Finally, in Fig. 4(d), where the sharp surface peak splits into two separated peaks whose amplitudes are only around 25% of that of the original Rayleigh wave peak.

The results of numerical simulation demonstrated strong lateral focusing of elastic waves at the epicenter with waves generated by a ring-shaped light source. The calculated results show that the elastic waves are narrowly confined near the epicentral axis. Thus, effective focusing in depth of the elastic waves can be achieved with this simple configuration. Furthermore, the waves are not narrowly focused at a single depth, which can facilitate the process of locating defects at unknown depths. Strong converging waves may be useful for detection of oriented flat cracks and flaws.

X. Ni is the author to whom the correspondence should be addressed, his e-mail address is nxw@mail.njust.edu.cn.

## References

1. C. E. Scruby and L. E. Drain, *Laser Ultrasonics Techniques and Application* (Adam Hilger, New York, 1990).
2. S. J. Davis, C. Edwards, G. S. Taylor, and S. B. Palmer, J. Phys. D: Appl. Phys. **26,** 329 (1993).
3. F. A. McDonald, Appl. Phys. Lett. **56,** 230 (1990).
4. C. B. Scruby, R. J. Dewhurst, and S. B. Palmer, J. Appl. Phys. **51,** 6210 (1980).
5. C. K. Jen, P. Cielo, J. Bussiere, and F. Nadeau, Appl. Phys. Lett. **46,** 241 (1985).
6. R. J . von Gutfeld and D. R. Vigliotti, Appl. Phys. Lett. **42,** 1018 (1983).
7. M.-H. Noroy, D. Royer, and M. Fink, Appl. Phys. Lett. **63,** 3276 (1993).
8. K. Yamanaka, Y. Nagata, and T. Koda, Appl. Phys. Lett. **58,** 1591 (1991).
9. M.-H. Noroy, D. Royer, and M. Fink, J. Acoust. Soc. Am. **94,** 1934 (1993).
10. X. Wang, M. G. Littman, J. B. McManus, M. Tadi, Y. S. Kim, A. Askar, and H. Rabitz, J. Appl. Phys. **80,** 4274 (1996).
11. B. Q. Xu, Z. H. Shen, X. W. Ni, J. Lu, S. Y. Zhang, International J. of Heat and Mass Transfer **46,** 4963 (2003).
12. B. Q. Xu, Z. H. Shen, X. W. Ni, and J. Lu, J. Appl. Phys. **95,** 2116 (2004).
13. B. Q. Xu, Z. H. Shen, X. W. Ni, J. Lu, and Y. W. Wang, J. Appl. Phys. **95,** 2109 (2004).